Two-component membrane material properties and domain formation from dissipative particle dynamics

G. Illya,[a] R. Lipowsky, and J. C. Shillcock
Max Planck Institute of Colloids and Interfaces, D-14424 Potsdam, Germany

(Received 13 June 2006; accepted 17 August 2006; published online 21 September 2006)

The material parameters (area stretch modulus and bending rigidity) of two-component amphiphilic membranes are determined from dissipative particle dynamics simulations. The preferred area per molecule for each species is varied so as to produce homogeneous mixtures or nonhomogeneous mixtures that form domains. If the latter mixtures are composed of amphiphiles with the same tail length, but different preferred areas per molecule, their material parameters increase monotonically as a function of composition. By contrast, mixtures of amphiphiles that differ in both tail length and preferred area per molecule form both homogeneous and nonhomogeneous mixtures that both exhibit smaller values of their material properties compared to the corresponding pure systems. When the same nonhomogeneous mixtures of amphiphiles are assembled into planar membrane patches and vesicles, the resulting domain shapes are different when the bending rigidities of the domains are sufficiently different. Additionally, both bilayer and monolayer domains are observed in vesicles. We conclude that the evolution of the domain shapes is influenced by the high curvature of the vesicles in the simulation, a result that may be relevant for biological vesicle membranes.
 [DOI: 10.1063/1.2353114]

I. INTRODUCTION

Biological cells are surrounded by a plasma membrane which controls the interface between the cell and its environment. This membrane is composed of proteins, lipids, and partially carbohydrates. Membrane-bounded organelles, such as vesicles, are also abundant within the cell, and the diameter of such vesicles can be as small as 40 nm. The most common lipid components in biomembranes are phospholipids, which are amphiphilic molecules possessing a hydrophilic headgroup and, usually, two hydrophobic tails. Phospholipids vary greatly in the composition of their headgroup, and the length and saturation of their tails. Experimental studies have clearly demonstrated that dissimilar phospholipids do not mix ideally[1–6] when the lipids composing the mixture have different chain melting temperatures. This temperature depends on the lipid hydrophobic chain lengths and the unsaturation of the chains, and these properties in turn influence the preferred area per molecule for each lipid type, and the packing of the lipid chains in the hydrophobic core of the bilayer. By changing the temperature or the composition, a mixture of two phospholipids with different melting temperatures may undergo lateral phase separation leading to the formation of domains.[5,6]

Beside numerous experimental works on the nonideal mixing of lipid bilayers, there are also measurements of the bending rigidity of heterogeneous membranes which indicate an explicit dependence of this material property on the membrane composition.[7–11]

Various theoretical and simulation models of mixed systems as a function of composition have also been developed. For simplicity, these models have mainly focused on two-component monolayers and bilayers. Szleifer *et al.*[12,13] and Gonzalez[14] have calculated the bending rigidity of two-component bilayers as a function of composition for various amphiphile chain lengths. Atomistic simulation techniques have been used to study the effect of single chain surfactants on mixed bilayers[15,16] and to determine the equilibrium packing parameter and chain order as a function of lipid composition.[17,18] Coarse-grained simulation techniques, which require far less computational resources than atomistic ones, have also been used to measure the material properties of binary mixtures of bilayers and monolayers.[19–21]

In this study, we use the dissipative particle dynamics simulation technique[22,23] to study bilayers composed of a mixture of two kinds of amphiphile. This technique has previously been used to extract the material properties of single-component bilayers composed of amphiphiles with symmetric and asymmetric tails,[24,25] and also to simulate various membrane-related processes, such as pore formation in amphiphilic bilayers,[26] self-assembly of vesicles,[27] phase separation in vesicles,[28,29] and vesicle budding.[30] It has also been used to explore the phase behavior of lipids[31] and the effects of surfactant packing at an oil-water interface.[32] Using this technique, we explore the dependence of the area stretch modulus and corresponding bending rigidity of binary mixture bilayers on their composition for various amphiphile packing parameters and tail lengths. We find that amphiphiles with different equilibrium packing areas do not mix homogeneously, and the resulting domain shapes are different in planar membrane patches and vesicles, which indicates that the vesicle curvature influences the domain evolution. This result may be significant for the behavior of vesicles in cellular processes.

[a]Present address: Max Planck Institute for Polymer Research, Mainz, Germany. Electronic mail: illya@mpip-mainz.mpg.de

II. DISSIPATIVE PARTICLE DYNAMICS SIMULATION METHOD

Dissipative particle dynamics (DPD) is a particle based simulation method, where each particle/bead has a mass m_0 and experiences three forces with those of its neighbors within the range d_0. The bead coordinates evolve in time under their mutual interactions according to Newton's laws of motion. The conservative force takes the form

$$\mathbf{F}_{ij}^{C} = a_{ij}(1 - r_{ij}/d_0)\hat{\mathbf{r}}_{ij}, \tag{2.1}$$

for $r_{ij} < d_0$, and zero otherwise. Here a_{ij} is the maximum repulsion between bead types i and j which are separated by a distance of r_{ij}, and $\hat{\mathbf{r}}_{ij}$ is the unit vector pointing from bead j to bead i. Additionally, dissipative and random forces are used to apply a thermostat to the system that ensures its evolution towards a Boltzmann-distributed equilibrium state. The dissipative force is of the form

$$\mathbf{F}_{ij}^{D} = -\gamma_{ij}(1 - r_{ij}/d_0)^2(\hat{\mathbf{r}}_{ij} \cdot \mathbf{v}_{ij})\hat{\mathbf{r}}_{ij}, \tag{2.2}$$

for $r_{ij} < d_0$, and zero otherwise, where γ_{ij} and $\mathbf{v}_{ij}$ are the dissipation strength and relative velocity between beads i and j, respectively. Finally, the random force is

$$\mathbf{F}_{ij}^{R} = \sqrt{2\gamma_{ij}k_BT}(1 - r_{ij}/d_0)\zeta_{ij}\hat{\mathbf{r}}_{ij}, \tag{2.3}$$

for $r_{ij} < d_0$, and is pairwise symmetric for all pairs of interacting beads. Here, ζ_{ij} is a uniform random variable that satisfies $\langle \zeta_{ij}(t) \rangle = 0$ and $\langle \zeta_{ij}(t)\zeta_{i'j'}(t') \rangle = (\delta_{ii'}\delta_{jj'} + \delta_{ij'}\delta_{ji'})\delta(t-t')$. Beads are assembled into amphiphilic molecules by tying them together with Hookean springs with the potential

$$U_2(i, i+1) = 1/2k_2(|\hat{\mathbf{r}}_{i,i+1}| - l_0)^2, \tag{2.4}$$

where the spring constant and unstretched bond length may be determined by comparing the end-to-end length of the model amphiphile with the actual molecular length. In order to represent the noninterdigitated state of typical lipid bilayers, it has been found necessary to add a chain stiffness potential to the amphiphiles' tails, U_3, where

$$U_3(i-1, i, i+1) = k_3[1 - \cos(\theta - \theta_0)], \tag{2.5}$$

in which the bending stiffness and preferred angle are chosen so as to produce a stable bilayer.[24,33] We consider amphiphiles with symmetric tails, which we model using the general architectures $H_m(T_n)_2$, where n is the number of hydrophobic beads in each tail and the headgroup contains m hydrophilic beads, see Fig. 1.

All simulations are carried out in the *NVT* ensemble at a reduced temperature $k_BT = 1$, and the actual dimensions of the box are chosen appropriately for each systems as described in the Results. The bilayer or vesicle is preassembled in the box and the remaining free volume filled with water particles to the desired density $\rho d_0^3 = 3$. All the results we present are taken from near-tensionless systems. This state was obtained by performing several runs with different numbers of amphiphiles at a constant box size to locate the system in which the bilayer's mean surface tension was close to zero. We have used the equilibrium area per amphiphile at the bilayer's tensionless state and the in-plane diffusion coefficient to extract the length and time scales for the simulations. The "standard" amphiphile architecture $H_3(T_6)_2$, which represents a typical phospholipid such as dimyristoylphosphatidylcholine (DMPC) with two to three methyl groups represented by one DPD tail bead, has equilibrium area per amphiphile about $\sim 1.262 \pm 0.001 (d_0)^2$. The experimental value[34] for the equilibrium area per molecule of DMPC in a bilayer is 0.6 nm^2. Comparing these two values results in $d_0 \approx 0.7$ nm. The time scale is extracted from the in-plane diffusion coefficient of the amphiphiles by fitting the mean square displacement (MSD) at large times. Taking a typical diffusion value for a DMPC molecule as[35] 5 $\mu\text{m}^2/\text{s}$ and comparing with the $H_3(T_6)_2$ amphiphile diffusion coefficient obtained from the simulation, the time scale of the simulation is found to be $t_0 = 0.46$ ns.

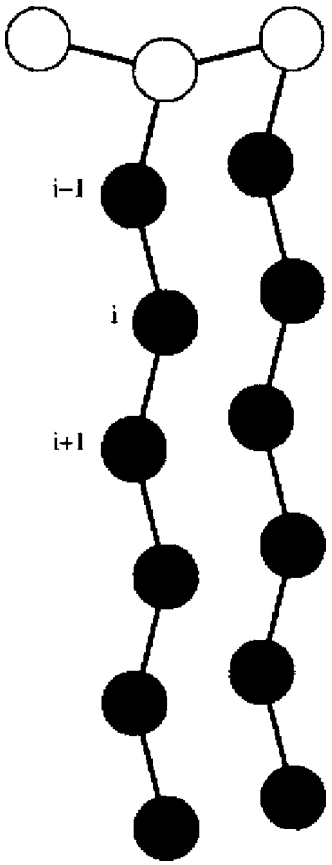

FIG. 1. Cartoon of the "standard" amphiphile architecture $H_3(T_6)_2$ used in this work.

In each simulation, the first 50 000 steps are discarded and observable averages are constructed from at least 1000 independent samples. The equations of motion are integrated using a velocity-Verlet scheme.[36] Using the values given above for the intrinsic DPD length ($d_0 = 0.7$ nm) and time ($t_0 = 0.46$ ns) scales, and an integration time step of $dt = 0.02t_0$ to ensure stability of the integrator, one simulation of 10^5 steps is equivalent to $10^5 \times 0.02 \times 0.46$ ns $= 0.9$ μs of real time, and requires 80 CPU hours on a single-processor Pentium system.

TABLE I. The conservative repulsion parameters a_{ij} for the three bead types used in the A, B amphiphile model. The head and tail beads composing the lipids are denoted by H and T, and the water beads by W. The amphiphile species are identified by the subscripts A and B.

	H_A	T_A	H_B	T_B	W
H_A	40	50	40	50	35
T_A	50	25	50	25	75
H_B	40	50	20	50	35
T_B	50	25	50	20	75
W	35	75	35	75	25

III. RESULTS

A. Nonhomogeneous mixture of $H_3(T_6)_2$ amphiphiles

In this subsection, we present the domain formation and the material parameters of a two-component bilayer composed of amphiphiles with an identical architecture [$H_3(T_6)_2$, denoted by A and B], but different preferred packing areas. The nonbonded bead-bead interaction parameters for the amphiphiles in the mixture are shown in Table I. The key difference between the A and B amphiphiles is that the conservative repulsion of two tail beads in amphiphile B is smaller than that of tail beads in amphiphile A, and also smaller than the repulsion between tail beads from the two amphiphiles. This choice is intended to mimic the ability of long, saturated hydrocarbon chains in lipids to pack somewhat closer together than chains that contain one or more double bonds, and to make the B amphiphiles phase separate from amphiphile A. In order to guarantee a stable single-component bilayer composed of amphiphile B, the small tail-tail repulsion has to be balanced by a small head-head repulsion. The cross head-head and tail-tail repulsions were chosen to be the same as the self-head-head and -tail-tail repulsions of amphiphile A since both of the amphiphiles have the same tail length. The choice of this parameter set is motivated by the material properties of single-component bilayers composed of $H_3(T_6)_2$ amphiphiles presented in our previous work.[25]

Our parameter set is quite different from those of two other recent DPD studies[28,30] that also explored the phase separation of binary mixtures of amphiphiles. In those studies, the cross tail-tail repulsion of the two types of amphiphile is set larger than the self-repulsion of tail beads in the same amphilphile, and it is this large repulsion that drives phase separation of the two species.

Unless otherwise stated, the planar bilayer is preassembled in a simulation box with dimensions $L_x=24$, $L_y=40$, and $L_z=32$. A rectangular plane in the direction of x and y axes has been chosen as the plane of the bilayer in order to reduce the influence of the symmetry of the simulation box on the domain patterns. Figure 2 shows the snapshots of the phase separation process of the two coexisting phases and the associated time-dependent growth of the domains in a planar bilayer composed of 944 amphiphiles A and 630 amphiphiles B. We start the simulation with a random configuration; and after 50 000 DPD steps the amphiphiles are completely separated and domains with irregular shapes are formed. As time passes, small domains coalesce to form larger domains. We have observed only circular domains of

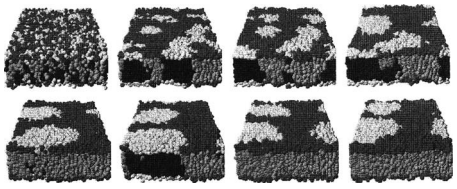

FIG. 2. Phase separation of amphiphile A (denoted by red heads, $x_A=0.6$) and amphiphile B (denoted by yellow heads, $x_B=0.4$) at $k_BT=1$, starting from random configuration to 400 000 DPD steps. The simulation box and water beads are invisible for clarity.

amphiphile B in five independent simulations of this mixture composition. The tensionless bilayers shown in Fig. 2 have a projected area per amphiphile $A_{\mathrm{pr}}/d_0^2=1.22$.

Figure 3 shows the equilibrium domain shapes in planar bilayers as a function of amphiphile B's concentration at 400 000 DPD steps. At amphiphile B concentration $x_B=0.1$, small circular domains of this amphiphile as shown in Fig. 3(a) are formed. Increasing the concentration of this amphiphile up to $x_B=0.3$ leads to the formation of circular domains with increasing size [Fig. 3(b)]. Striped domains are seen at a 50:50 mixture of both amphiphiles [Fig. 3(c)]. Finally, at $x_B=0.7$, two inverted circular domains composed of amphiphile A are formed [Fig. 3(d)].

Note that as seen in all snapshots, commensurate domains are formed in both of the monolayers, which indicates that there is a strong coupling between the amphiphiles in both of the monolayers, as has been observed in several experimental studies.[5,6,38,39] The coupling that we find in our simulations is primarily driven by the 20% reduction in the tail-tail repulsion parameter of amphiphile B, $a_{TT}d_0/k_BT=20$, compared to that of amphiphile A, which leads to closer packing of the amphiphile's tails. We have measured the surface tension of the bilayers as a function of amphiphile's packing area and calculated their area stretch modulus around the zero crossing point using the relation[33]

$$\Sigma(A,n_1)\approx K[A_{\mathrm{pr}}-A_0(n_1)]/A_0(n_1), \tag{3.1}$$

where Σ is the bilayer surface tension, A_0 is the projected area at zero surface tension, K is the area stretch modulus, and n_1 is the amphiphile's tail length. The bending rigidity of the bilayer can then be estimated from the relation[37]

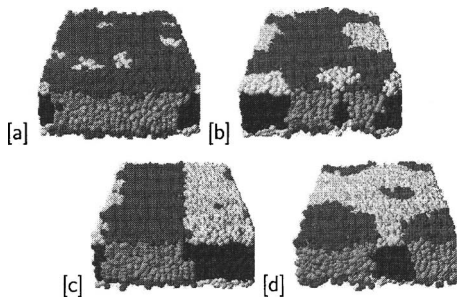

FIG. 3. Phase separation of amphiphiles A (denoted by red heads) and B (denoted by yellow heads) for various mixture compositions in the tensionless state, at 400 000 DPD steps [(a) $x_B=0.1$, (b) $x_B=0.3$, (c) $x_B=0.5$, and (d) $x_B=0.7$]. The simulation box and water beads are invisible for clarity.

TABLE II. We summarize here the material properties of bilayers composed of a mixture of amphiphiles *A* and *B* as a function of amphiphile *B* concentration. The equilibrium area per amphiphile and bilayer width in the tensionless state are displayed in columns 2 and 3, and the area stretch modulus and bending rigidity in columns 4 and 5. The bending rigidity is calculated using Eq. (3). The results in this table are obtained from averaging over five independent simulations for each projected area. Note that K was calculated using only points around the tensionless state, and by taking k_BT as room temperature and $d_0=0.7$ nm.

x_B	A_0/Nd_0^2	$\langle \ell_{me} \rangle / d_0$	K (dyn/cm)	κ (k_BT)
0	1.262	6.79±0.01	736±49	84±6
0.1	1.255	6.79±0.04	850±51	97±6
0.3	1.23	6.8±0.04	1036±53	118±6
0.5	1.21	6.81±0.04	1114±41	127±5
0.7	1.187	6.8±0.05	1186±49	135±6
0.9	1.165	6.83±0.05	1218±39	140±5
1.0	1.155	6.84±0.01	1264±16	146±2

$$\kappa = K\ell_{me}^2/48, \tag{3.2}$$

where ℓ_{me} is the bilayer membrane thickness. Since amphiphile *B* has smaller head-head and tail-tail repulsion parameters, $a_{HH}d_0/k_BT=a_{TT}d_0/k_BT=20$, than amphiphile *A*, a single-component bilayer of this amphiphile has a bending rigidity almost twice as large as a bilayer composed solely of amphiphile *A*, reflecting the closer packing of the *B* amphiphile tails. Table II shows the variation of the material properties of a bilayer containing *A* and *B* amphiphiles as the fraction of amphiphile *B* is increased from 0% to 100%. We see that upon replacement of 50% of amphiphile *A* with amphiphile *B*, the bending rigidity of the bilayer increases 36%, indicating that amphiphile *B* makes the bilayer more rigid. The area per amphiphile for the bilayer at its tensionless state also decreases slightly as the concentration of amphiphile *B* increases, also indicating the closer packing of the tails of amphiphile *B* compared to those of amphiphile *A*. Since amphiphiles *A* and *B* have the same tail length, the bilayer widths of various compositions of these amphiphiles are almost constant, as shown in Table II.

From Figs. 4 and 5, we can see that the area stretch modulus and bending rigidity of the bilayer increase monotonically as the concentration of amphiphile *B* increases. This result is in a fair agreement with the theoretical prediction of bending rigidity of a mixture of lipids of different chain stiffnesses, but same length and volume.[14] In Ref. 14, they studied the material properties of amphiphilic molecules containing fluorocarbon (CF_2) groups, which form stiffer chains than those composed of CH_2 groups, in the sense that their *trans*-gauge energy is much larger than that of hydrocarbons. They find that the the stiffer chains increase the bending rigidity of the aggregate and slightly decrease the optimal packing area.

Quadratic fits to the data for the area stretch modulus K, as displayed in Fig. 4, and the bending rigidity κ, as shown in Fig. 5, yield their functional dependence on the concentration x_B of amphiphile *B* as given by

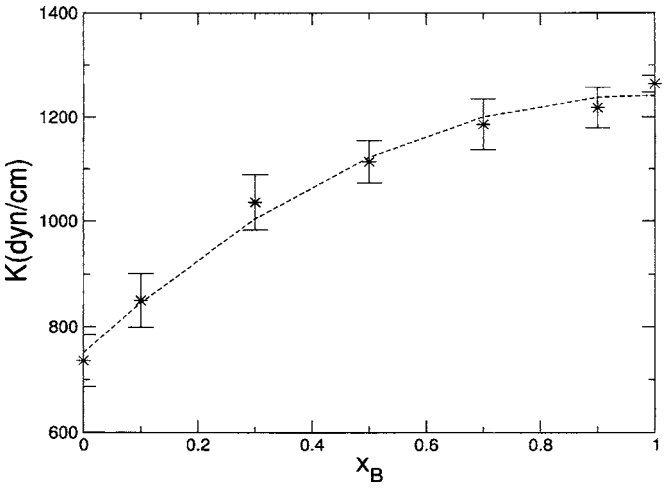

FIG. 4. Bilayer area stretch modulus as a function of amphiphile *B* concentration, mixed with amphiphile *A*. The dashed line is a quadratic fit of the area stretch modulus.

$$K = 751.24 + 995.56x_B - 505.34x_B^2 \tag{3.3}$$

and

$$\kappa = 85.927 + 110.09x_B - 52.759x_B^2. \tag{3.4}$$

We have also observed phase separation in bilayer vesicles composed of a binary mixture of lipids *A* and *B*. Performing simulations of phase separation on a vesicle removes the periodic boundary conditions that may modify the domain equilibrium state in planar bilayer simulations. However, the curvature of the vesicle may now influence the dynamics of domain formation, and our results should be compared with small, unilamellar vesicles with diameters around 20 nm. In this way, the small vesicles reveal the effects of large curvature on the domain growth, while the planar membranes represent the limiting case of infinite-diameter (or zero curvature) vesicles. The vesicle is initially preassembled with a diameter of $d/d_0=32$ in a simulation box size $(52d_0)^3$ filled with water. The number of amphiphiles *A* and *B* is varied and has been calculated from dividing the vesicle's area with the equilibrium area per amphiphile A_0/d_0^2 obtained

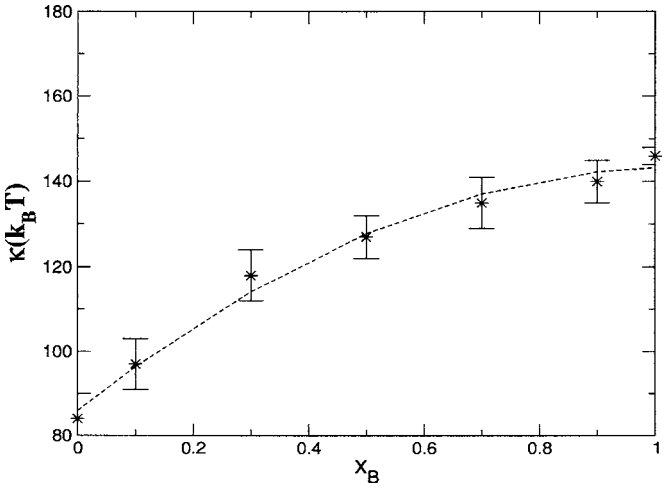

FIG. 5. Bending rigidity as a function of amphiphile *B* concentration, mixed with amphiphile *A*. The dashed line is a quadratic fit of the bending rigidity.

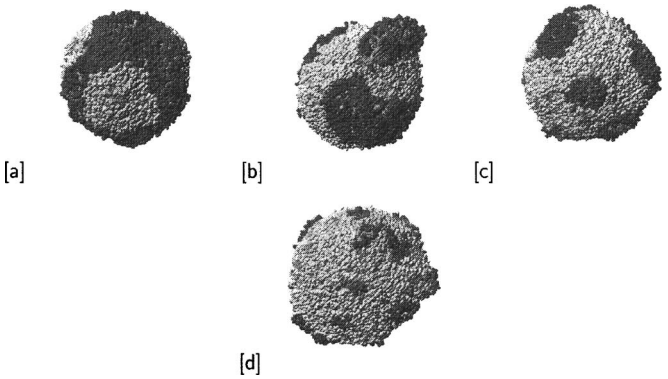

FIG. 6. Phase separation of amphiphiles A (denoted by red heads) and B (denoted by yellow heads) at (a) $x_B=0.1$, (b) $x_B=0.5$, (c) $x_B=0.7$, and (d) $x_B=0.9$. The similarity between the shapes of the domains formed in these vesicles for a given mixture composition and those formed in planar membranes of equivalent composition shown in Fig. 3 is evident.

from the surface tension measurements for each mixture composition on planar bilayers. There are initially 2572 water beads inside the vesicle, and none of them are observed to leave the vesicle during the simulations, which implies that the vesicle is impermeable to water on the time scale of the simulations. Figure 6 shows a series of images of domain formation on vesicles as a function of amphiphile B's concentration at 400 000 DPD steps. At $x_B=0.3$, circular domains of amphiphile B are found [Fig. 6(a)]. At 1:1 mixture, striped domain of amphiphile B is observed [Fig. 6(b)]. Increasing the concentration of amphiphile B to $x_B=0.7$ and $x_B=0.9$ leads to formation of inverted circular domains composed of amphiphile A with different sizes depending on the mixture composition [Figs. 6(c) and 6(d)].

Comparing the results shown in Figs. 3 and 6 shows that the typical domain shapes in vesicles at different amphiphile concentrations are similar to those in planar bilayers.

B. Homogeneous mixture of $H_3(T_8)_2$ and $H_3(T_6)_2$ amphiphiles

In order to compare the material properties of nonhomogeneous and homogeneous mixtures of two different amphiphiles, we present in this section the material properties of homogeneous mixtures of $H_3(T_6)_2$ (denoted by A) and $H_3(T_8)_2$ (denoted by C) amphiphiles. In these mixtures, the preferred packing area of amphiphile C is close to that of amphiphile A. The interaction parameters for amphiphiles A and C are described below, where the cross head-head repulsion parameter between these two types of amphiphiles is chosen to be in between their self-interactions (see Table III). These interactions and the rest of the simulation parameters are chosen so as to mimic the material properties of typical lipid membranes, which have been studied in our previous works.[24,25] Note that in this section the planar bilayers are preassembled in a simulation box size of $(32d_0)^3$.

TABLE III. The conservative repulsion parameters a_{ij} for the three bead types used in the A, C amphiphile model. The symbols H, T, and W are the same as in Table I. and the amphiphiles are identified by the subscripts A and C.

	H_A	T_A	H_C	T_C	W
H_A	40	50	45	50	35
T_A	50	25	50	25	75
H_C	45	50	50	50	35
T_C	50	25	50	25	75
W	35	75	35	75	25

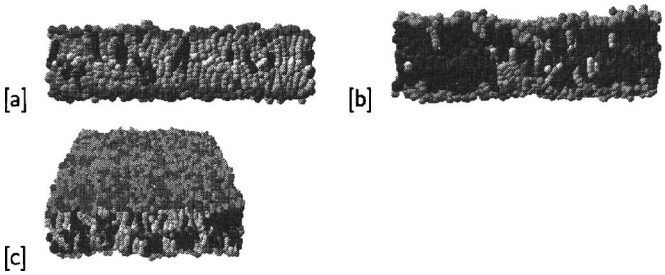

FIG. 7. Snapshots of various mixtures of amphiphiles A (denoted by red heads, orange tails, and yellow tail ends) and C (denoted by green heads, blue tails, and purple tail ends), at (a) $x_C=0.1$ and (b) $x_C=0.9$, and at (c) 1:1 mixture. The amphiphiles mix ideally in the membrane. The tail ends corresponding to the last tail beads of the amphiphiles are colored differently to show the interdigitation between the upper and lower monolayers.

Figure 7 shows the homogeneous mixtures of $H_3(T_8)_2$ and $H_3(T_6)_2$ amphiphiles for various compositions. The presence of a small concentration of the longer amphiphiles in a bilayer composed of the shorter amphiphiles disrupts the bilayer structure, which decreases the bilayer stretch and bending rigidity (see Table IV), and vice versa. While for the 1:1 mixture, almost every $H_3(T_6)_2$ amphiphile is paired with one $H_3(T_8)_2$ amphiphile from the opposing monolayer. We note that the bending rigidity of the membrane with a 1:1 mixture of the two types of amphiphile is identical, within the error bars calculated from five independent simulations, to that of the pure shorter-chain amphiphile membrane.

For this homogeneous mixture, the area stretch modulus (Fig. 8) and bending rigidity (Fig. 9) show nonmonotonic dependencies on the composition, a result that is in fair agreement with several theoretical predictions[12–14] and previous coarse-grained molecular dynamics simulations of two-component lipid bilayers[19] that measured the membrane's bending rigidity from its shape fluctuations. Equa-

TABLE IV. We summarize here the material properties of bilayers composed of a mixture of amphiphiles A and C as a function of amphiphile C concentration. The equilibrium area per amphiphile and bilayer width in the tensionless state are displayed in columns 2 and 3, and the area stretch modulus and bending rigidity in columns 4 and 5. The bending rigidity is calculated using Eq. (3). The results in this table are obtained from averaging over five independent simulations for each projected area. Note that K was calculated using only points around the tensionless state, and by taking k_BT as room temperature and $d_0=0.7$ nm.

x_C	A_0/Nd_0^2	$\langle \ell_{me} \rangle / d_0$	K (dyn/cm)	κ (k_BT)
0	1.262	6.79±0.01	736±49	84±6
0.1	1.278	7.09±0.02	569±34	68±4
0.3	1.275	7.07±0.03	579±19	72±2
0.5	1.265	8.46±0.02	679±27	85±3
0.7	1.257	8.5±0.02	758±41	134±7
0.9	1.253	8.62±0.02	1005±35	178±7
1.0	1.252	8.88±0.01	1186±43	231±8

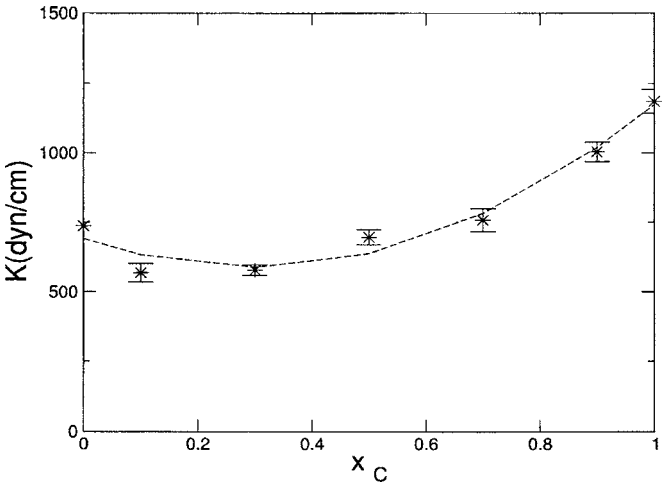

FIG. 8. Bilayer area stretch modulus as a function of amphiphile C concentration, mixed with amphiphile A. The dashed line is a quadratic fit of the area stretch modulus.

tions (3.5) and (3.6) show the quadratic fits of the area stretch modulus (Fig. 8) and bending rigidity (Fig. 9):

$$K = 690.88 - 691.28x_C + 1174.8x_C^2 \tag{3.5}$$

and

$$\kappa = 81.594 - 119.57x_C + 263.91x_C^2. \tag{3.6}$$

The minimum values of these material parameters are located in the relatively flat region between $x=0.1$ and $x=0.3$. We deduce (by looking at the snapshots) that the inclusion of long/short amphiphile into the bilayer of short/long amphiphile in homogeneous system disrupts its structure (the two monolayers become interdigitated), which decreases its area stretch modulus. This assumption is similar to that in the work of Szleifer *et al.*, where the long tail lipid dangling essentially free in the bilayer midplane causes the bending rigidity of the mixed system to be less than the corresponding pure systems. The bilayer thickness of this mixture increases as the concentration of the long amphiphile increases, while its equilibrium area per amphiphile is almost constant.

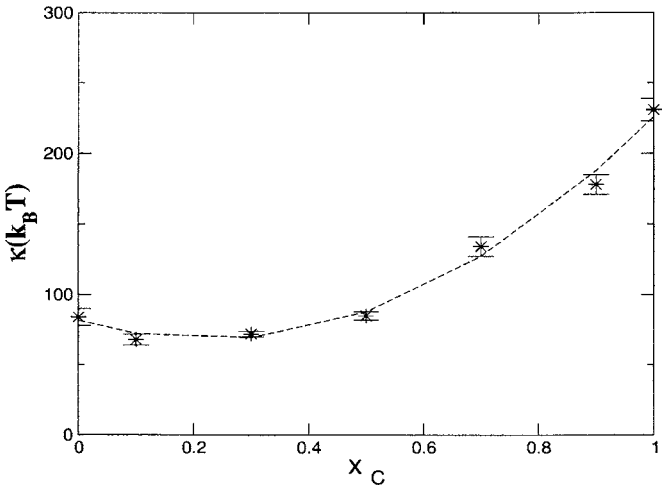

FIG. 9. Bending rigidity as a function of amphiphile C concentration, mixed with amphiphile A. The dashed line is a quadratic fit of the bending rigidity.

TABLE V. The conservative repulsion parameters a_{ij} for the three bead types used in the A, D amphiphile model. The symbols H, T, and W are the same as in Table I, and the amphiphiles are identified by the subscripts A and D

	H_A	T_A	H_D	T_D	W
H_A	40	50	45	50	35
T_A	50	25	50	25	75
H_D	45	50	20	50	35
T_D	50	25	50	20	75
W	35	75	35	75	25

C. Nonhomogeneous mixture of $H_3(T_8)_2$ and $H_3(T_6)_2$ amphiphiles

In this subsection, we present the material properties and domain shape evolution of nonhomogeneous mixtures of $H_3(T_8)_2$ and $H_3(T_6)_2$ amphiphiles. The phase separation of the mixtures has been simulated in the same way as the previous nonhomogeneous system (Sec. III A), by choosing the self-tail-tail interaction parameter of $H_3(T_8)_2$ amphiphile (denoted as D) to be smaller than that of $H_3(T_6)_2$ amphiphile (denoted as A) and of the cross interactions (see Table V). The rest of the interaction parameters are the same as in the previous system (Sec. III A).

We found that the domain shape evolution of this mixture in planar bilayers is similar to that fo the nonhomogeneous mixture of amphiphiles A and B, as shown in Fig. 3.

Figure 10 shows the domain shape evolution of this mixture in vesicles with diameter $d/d_0=32$, as a function of amphiphile's composition.

The domains composed of amphiphile D in vesicles are more rectangular than circular compared to those in planar bilayers because they are rigid, similar to solid plates (see the bending rigidity estimations in Table VI). Their rigidity requires them to be stretched locally in order to deform smoothly onto the spherical surface, and the energy cost of this deformation can be reduced for longer, thinner domains. Figure 11 shows the cross sections through the vesicles, where at $x_D=0.1$, the domains are formed on both of the monolayers, while at $x_D=0.9$, the vesicle is very rigid, and the striped domains are formed only on one of the monolayers. Taking the time scale of the simulation as $t_0=0.46$ ns and the bead diameter $d_0=0.7$ nm, the lateral diffusion coefficients of amphiphiles A and D at 1:1 mixture shown in Fig. 10 are 8.5 and 7.4 $\mu m^2/s$, respectively. The small difference in the diffusion coefficient between amphiphiles A and D for the equal concentration in vesicle shown in Fig. 10 indicates that the two amphiphiles are in the same state, i.e., liquid state. The area stretch modulus calculation for various compositions of this mixture is shown in Table VI. Note that a single-component bilayer of amphiphile D has bending rigidity $\kappa=469\pm12k_BT$ which is five times larger than that of single-component bilayer composed of amphiphile A ($\kappa=84\pm6k_BT$).

The quadratic fits of the area stretch modulus (Fig. 12) and bending rigidity (Fig. 13) are shown as follows:

$$K = 694.92 + 161.43x_D + 1413.8x_D^2 \tag{3.7}$$

and

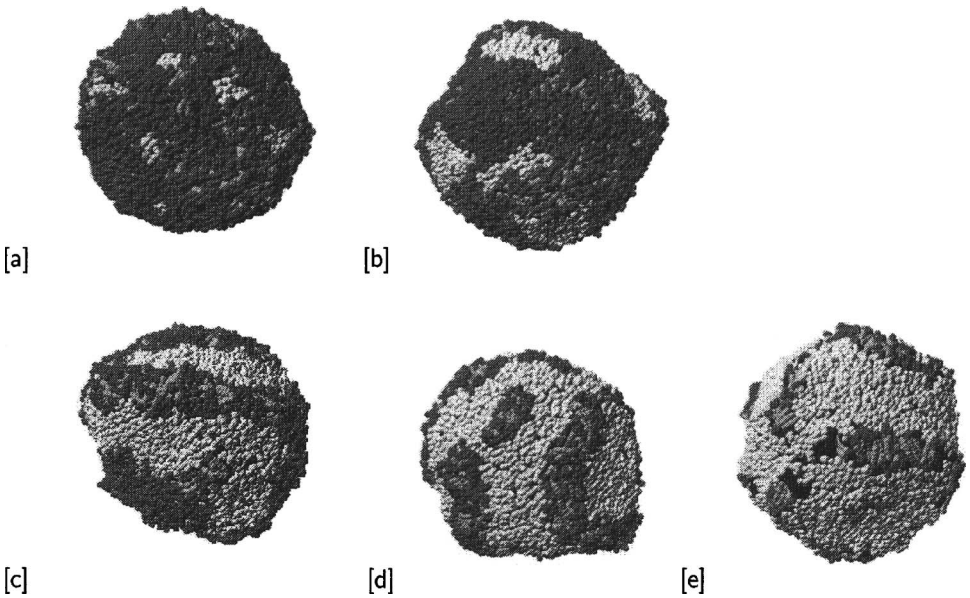

FIG. 10. Phase separation of various mixtures of amphiphile A (denoted by red heads) and amphiphile D (denoted by yellow heads) at 200 000 DPD steps [(a) $x_D=0.1$, (b) $x_D=0.3$, (c) $x_D=0.5$, (d) $x_D=0.7$, and (e) $x_D=0.9$].

$$\kappa = 81.185 - 14.604x_D + 374.27x_D^2. \tag{3.8}$$

The equilibrium area per amphiphile decreases and the bilayer thickness increases as the concentration of amphiphile D increases in the system. Comparing this mixture with the nonhomogeneous mixture of amphiphiles A and B, in this mixture, the area stretch and bending rigidity increase drastically at the concentration above $x_D=0.1$.

At the concentration below $x_D=0.1$, the inclusion of long amphiphile D disrupts the bilayer structure, because they are not paired with each other in both of the monolayers, while at the concentration above $x_D=0.1$, almost each of this amphiphile is paired with another one from the opposing monolayer, which is found to strengthen the bilayer. Our result on bending rigidity for this mixture is similar to that of Monte Carlo simulations of two rods with different lengths in a constant area ensemble.[20]

IV. CONCLUSIONS

We have used dissipative particle dynamics simulations to explore the dependence of the material properties of two-component amphiphilic bilayers on their composition and the structure of the amphiphiles. The formation of domains in the mixed membranes has also been investigated. We have varied the tail length of the amphiphiles and their preferred area per molecule. The latter quantity is related to the degree of unsaturation in natural lipids, and we modulate its value by making modest changes in the tail-tail interaction parameters. We find that the amphiphiles can phase separate for quite small changes, which are of the order of 10%, in their preferred area per molecule. Furthermore, we find that increasing the amphiphile tail length and reducing their preferred packing area modestly are sufficient to increase the membrane stiffness by up to a factor of 5 depending on the composition. Our results are complementary to a recent paper,[29] which studied domain formation and budding in two-component vesicles, where a large repulsion between the tails of amphiphiles with identical structures was used to drive the phase separation. The physical origin of this large repulsion between identical hydrocarbon tails is not apparent, but it drives two lipid types to phase separate. The authors follow the evolution of the domains, measure their geometric properties including their mean radius and perimeter length, and find that hydrodynamic forces influence the coarsening dynamics at all time scales. They also observe budding of the domains for certain parameter values, and the buds are seen to detach from the parent vesicle.

In a nonhomogeneous mixture of $H_3(T_6)_2$ amphiphiles, where one of the amphiphiles has a slightly smaller preferred area per molecule, the difference in packing leads to a mono-

TABLE VI. We summarize here the material properties of bilayers composed of a mixture of amphiphiles A and D as a function of amphiphile D concentration. The equilibrium area per amphiphile and bilayer width in the tensionless state are displayed in columns 2 and 3, and the area stretch modulus and bending rigidity in columns 4 and 5. The bending rigidity is calculated using Eq. (3). The results in this table are obtained from averaging over five independent simulations for each projected area. Note that K was calculated using only points around the tensionless state, and by taking k_BT as room temperature and $d_0=0.7$ nm

x_D	A_0/Nd_0^2	$\langle \ell_{me} \rangle / d_0$	K (dyn/cm)	κ (k_BT)
0	1.262	6.79±0.01	736±49	84±6
0.1	1.26	6.94±0.01	566±27	67±7
0.3	1.23	7.09±0.02	1050±41	130±5
0.5	1.207	7.83±0.02	1169±51	175±5
0.7	1.185	8.25±0.02	1406±23	248±4
0.9	1.165	8.5±0.01	1836±60	336±8
1.0	1.157	8.9±0.01	2413±61	469±7

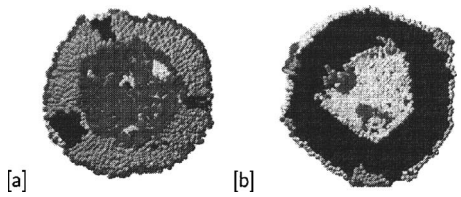

FIG. 11. Cross section through the vesicles at (a) $x_D=0.1$ and (b) $x_D=0.9$, respectively. In case (a), the domains extend over both monolayers, whereas in case (b) the domains are observed in one of the monolayers only.

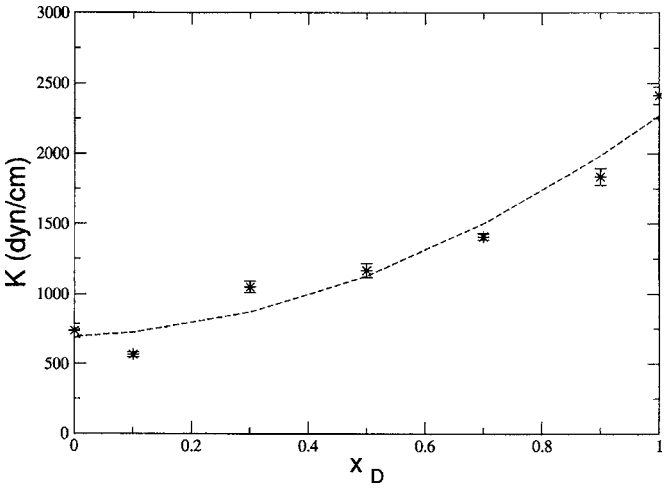

FIG. 12. Bilayer area stretch modulus as a function of amphiphile *D* concentration, mixed with amphiphile *A*. The dashed line is a quadratic fit of the area stretch modulus.

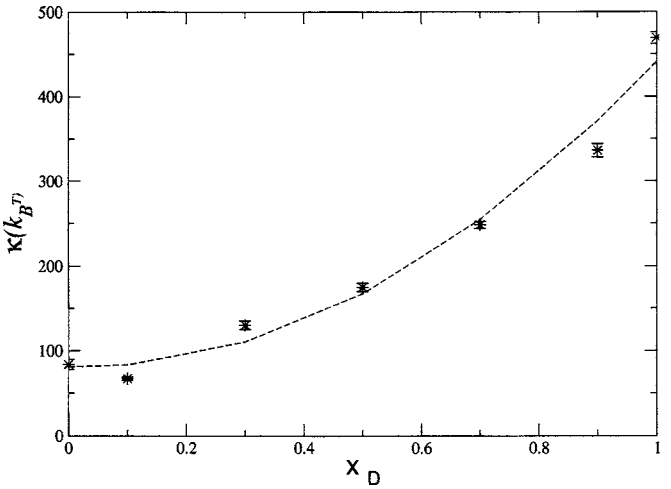

FIG. 13. Bending rigidity as a function of amphiphile *D* concentration, mixed with amphiphile *A*. The dashed line is a quadratic fit of the bending rigidity.

tonic increase in the membrane's bending rigidity as the fraction of the amphiphile with the smaller preferred area per molecule increases, resulting in a modest factor-of-2 change for the membrane containing only amphiphiles with the smaller preferred area. In a homogeneous mixture of $H_3(T_6)_2$ and $H_3(T_8)_2$ amphiphiles, the membrane bending rigidity changes nonmonotonically as the fraction of the longer-chain amphiphile increases, at first decreasing and then increasing by a factor of 3 when all of the shorter-chain amphiphiles have been replaced by the longer ones. However, a nonhomogeneous mixture of these amphiphiles has a membrane rigidity about five times larger than the single-component $H_3(T_6)_2$ bilayer. These results show that increasing the amphiphile tail length alone, or reducing the preferred packing of one amphiphile species, is not as effective in increasing the membrane bending rigidity as making modest changes in both properties simultaneously. Because making small changes in several molecular properties is generally simpler than making a large change in any one property, this result may be used to modify the material properties of biological membranes, which are composed of a large number of different types of amphiphile.

The shape of the domains formed in planar bilayers of a nonhomogeneous mixture of amphiphiles with the same architecture, $H_3(T_6)_2$, but different preferred areas per molecule, changes with the membrane composition in a manner similar to those of a nonhomogeneous mixture of $H_3(T_8)_2$ and $H_3(T_6)_2$ amphiphiles (data not shown). Since the bending rigidity of a single-component $H_3(T_6)_2$ planar bilayer varies by only a factor of 2 for the two preferred packing areas we use, the domain shapes of this mixture in vesicles are similar to those in planar bilayers. However, domains formed of amphiphiles $H_3(T_8)_2$ in a mixture with $H_3(T_6)_2$, in which the bending rigidity of the domains is five times larger than that of the surrounding sea of shorter amphiphiles, adopt distinct shapes in planar membrane and vesicles. Whereas such domains in planar bilayers are approximately circular, the difficulty of bending the stiffer domains onto the highly curved surface of the vesicle drives them to lengthen and form thinner, elongated domains instead. This result shows that the curvature of vesicles formed of amphiphiles whose properties differ in physically realistic ways (small difference in tail length and small change in preferred area per molecule) is sufficient to influence the formation and shape of domains on length scales close to those of biologically relevant vesicles, such as synaptic vesicles.

[1] S. H. Wu and H. M. McConnell, Biochemistry **14**, 850 (1975).
[2] S. Mabrey and J. M. Sturtevant, Proc. Natl. Acad. Sci. U.S.A. **73**, 3862 (1976).
[3] D. A. Wilkinson and J. F. Nagle, Biochemistry **18**, 4244 (1979).
[4] M. B. Sankaram and T. E. Thompson, Biochemistry **31**, 8258 (1992).
[5] J. Korlach, P. Schwille, W. W. Webb, and G. W. Feigenson, Proc. Natl. Acad. Sci. U.S.A. **96**, 8461 (1999).
[6] L. A. Bagatolli and E. Gratton, Biophys. J. **79**, 434 (2000).
[7] J. M. di Meglio, M. Dvolaitzky, and C. Taupin, J. Phys. Chem. **89**, 871 (1985).
[8] C. R. Safinya, E. B. Sirota, D. Roux, and G. S. Smith, Phys. Rev. Lett. **62**, 1134 (1989).
[9] R. Dimova, H. G. Döbereiner, and R. Lipowsky, Eur. Biophys. J. **29**, 287 (2000).
[10] R. Dimova, H. G. Döbereiner, and R. Lipowsky, Biophys. J. **82**, 506 (2002).
[11] H. V. Ly and M. L. Longo, Biophys. J. **87**, 1013 (2004).
[12] I. Szleifer, D. Kramer, A. Ben-Shaul, D. Roux, and W. M. Gelbart, Phys. Rev. Lett. **60**, 1966 (1988).
[13] I. Szleifer, D. Kramer, A. Ben-Shaul, W. M. Gelbart, and S. A. Safran, J. Chem. Phys. **92**, 6800 (1990).
[14] A. P. Gonzalez, J. Chem. Phys. **120**, 11267 (2004).
[15] M. J. Schneider and S. E. Feller, J. Phys. Chem. B **105**, 1331 (2001).
[16] S. Bandyopadhyay, J. C. Shelley, and M. L. Klein, J. Phys. Chem. B **105**, 5979 (2001).
[17] A. H. de Vries, A. E. Mark, and S. J. Marrink, J. Phys. Chem. B **108**, 2454 (2004).
[18] A. A. Gurtovenko, M. Patra, M. Karttunen, and I. Vattulainen, Biophys. J. **86**, 3461 (2004).
[19] A. Imparato, J. C. Shillcock, and R. Lipowsky, Europhys. Lett. **69**, 650 (2005).
[20] G. Brannigan and F. L. H. Brown, J. Chem. Phys. **122**, 074905 (2005).
[21] L. Rekvig, B. Hafskjold, and B. Smit, J. Chem. Phys. **120**, 4897 (2004).
[22] P. J. Hoogerbrugge and J. M. V. A. Koelman, Europhys. Lett. **19**, 155 (1992).
[23] R. D. Groot and P. B. Warren, J. Chem. Phys. **107**, 4423 (1997).
[24] J. C. Shillcock and R. Lipowsky, J. Chem. Phys. **117**, 5048 (2002).
[25] G. Illya, R. Lipowsky, and J. C. Shillcock, J. Chem. Phys. **122**, 5048 (2005).
[26] R. D. Groot and K. L. Rabone, Biophys. J. **81**, 725 (2001).

[27] S. Yamamoto, Y. Maruyama, and S. Hyodo, J. Chem. Phys. **116**, 5842 (2002).
[28] M. Laradji and P. B. Sunil Kumar, Phys. Rev. Lett. **93**, 198105 (2004).
[29] M. Laradji and P. B. Sunil Kumar, J. Chem. Phys. **123**, 224902 (2005).
[30] S. Yamamoto and S. Hyodo, J. Chem. Phys. **118**, 7937 (2003).
[31] M. Kranenburg, M. Venturoli, and B. Smit, Phys. Rev. E **67**, 060901 (2003).
[32] L. Rekvig, M. Kranenburg, J. Vreede, B. Hafskjold, and B. Smit, Langmuir **19**, 8195 (2003).
[33] R. Goetz and R. Lipowsky, J. Chem. Phys. **108**, 7397 (1998).
[34] J. F. Nagle, R. T. Zhang, S. Tristram-Nagle, W. J. Sun, H. I. Petrache, and R. M. Suter, Biophys. J. **70**, 1419 (1996).
[35] G. Oradd, G. Lindblom, and P. W. Westerman, Biophys. J. **83**, 2702 (2002).
[36] M. P. Allen and D. J. Tildesley, *Computer Simulation of Liquids* (Clarendon, Oxford, 1987).
[37] R. Goetz, G. Gompper, and R. Lipowsky, Phys. Rev. Lett. **82**, 221 (1999).
[38] T. Baumgart, S. T. Hess, and W. W. Webb, Nature (London) **425**, 821 (2003).
[39] D. Scherfeld, N. Kahya, and P. Schwille, Biophys. J. **85**, 3758 (2003).